

MHD Mixed Convective Heat Transfer of a Micropolar Fluid Over an Unsteady Stretching Porous Wedge with Viscous Dissipation and Joule Heating

Tarikul Islam, Muhammad Minarul Islam*

Department of Mathematics, Bangabandhu Sheikh Mujibur Rahman Science and Technology University, Gopalganj, Bangladesh.

***Corresponding Author**

E-Mail Id: minarul_math@yahoo.com

ABSTRACT

This study investigate numerically heat and mass transfer characteristics of two dimensional unsteady MHD mixed convective flow of a micropolar fluid along a stretchin permeable wedge taking into account the effects of viscous dissipation and Joule heating with convective boundary condition. The governing partial differential equations are transferred into ordinary differential equations using a set of non-dimensional variables and solve them numerically by Nachtsheim-Swigert shooting iteration technique with sixth order Runge-Kutta method. Effects of non-dimensional governing parameters on velocity, microrotation and temperature profiles are presented through graphs and discussed from physical point of view. The local skin friction coefficient, plate couple stress and the rate of heat transfer is also investigated for the different values of the pertinent parameters. The results show that both the rate of share stress and the rate of heat transfer increase with the increase of Hartmann number and Eckert number for both suction and injection cases.

Keywords: Joule heating, viscous dissipation, MHD, suction/injection, wedge

INTRODUCTION

The importance of materials flow in industrial processing is increasing day by day. The copling between the rotation of each particles and the macroscopic velocity of the particles of the fluid is considered in micropolar fluid. To explanin the complex hydrodynamic behavior of micropolar fluid, the classical theories of continuum mechnics are inadequate. Animal bloods, extrusion of polymer fluids, glass fiber, colloidal suspensions, exotic lubricants, and solidification of liquid crystals are the world applications of micropolar fluid in various industrial and engineering processes. The Dynamics of micropolar originated from the theory of Eringen [1] and its extension to the micropolar fluids, developed by Eringen [2], which can be used to explain the characteristics in certain fluids such as colloidal

suspensions, porous rocks, exotic lubricants and polymeric fluids etc. So, it has become a popular area of research due to the applications in a number of processes that occurs in industry. The mass flow and heat transfer characteristics of micropolar fluids under different situations studied by many researchers, for example, El-Hakiem *et al.* [3] studied Joule heating effects on magnetohydrodynamic free convection flow of a micropolar fluid. Duwairi [4] studied viscous and Joule heating effects on forced convection flow from radiate isothermal porous surfaces. Mixed convection flow and heat transfer characteristics of fluid of exponential stretching surface with viscous dissipation was investigated by Partha *et al.* [5]. Ishak *et al.* [6] studied Falkner-Skan equation for flow past a moving wedge with suction or injection. The convective flows of micropolar fluids from radiate isothermal

porous surface with viscous dissipation and joule heating is investigated by Rahman [7]. Aissa and Mohammadein [8] studied Joule heating effects in a micropolar fluid past a stretching sheet with variable electric conductivity.

In industrial processes, the MHD boundary layer flow induced by stretching or shrinking wedge has various technical applications. Some of these applications include wire drawing, paper production, glass-fiber production, polymer sheet synthesis, continuous stretching of plastic films and artificial fibers etc. MHD flow and heat transfer of a non-Newtonian power-law fluid past a stretching sheet with suction or injection and viscous dissipation was studied by Kishan and Shashidar [9]. A local similarity solution of an unsteady MHD convective flow of a micropolar fluid past a continuously moving porous was investigated by Alam et al. [10]. Viscous dissipation and Joule heating on steady MHD flow and heat transfer of a Bingham fluid over a porous rotating disk in the presence of Hall and ion-slip currents was investigated by Osalusi *et al.* [11]. Su, Zheng, Zhang and J. Zhang [12] studied MHD mixed convective heat transfer over a permeable stretching wedge with thermal radiation and ohmic heating.

The aim of the present study is to investigate the unsteady MHD mixed convective boundary layer flow and heat transfer characteristics of micropolar fluid over a stretching wedge in the presence of viscous dissipation and Joule heating with convective surface boundary condition.

Continuity Equation:

$$\frac{\partial u}{\partial x} + \frac{\partial v}{\partial y} = 0$$

Momentum Equation:

$$\frac{\partial u}{\partial t} + u \frac{\partial u}{\partial x} + v \frac{\partial u}{\partial y} = \frac{\partial U}{\partial t} + U \frac{\partial u}{\partial x} + \nu_a \frac{\partial^2 u}{\partial y^2} + \frac{s}{\rho} \frac{\partial N}{\partial y} + g_0 \beta^* (T - T_\infty) - \frac{\sigma B_0^2}{\rho_\infty} (u - U) \quad (2)$$

Angular Momentum Equation:

MATHEMATICAL MODELING

Flow Analysis

We consider an unsteady, laminar, incompressible two dimensional MHD mixed convective flow of micropolar fluid past a permeable stretching wedge. $B=(0, B_0, 0)$ is the uniform magnetic field which is acting normal to the surface of the wedge. $\Omega = \beta\pi$ is the angle of the wedge and $u = \lambda U$ is the stretching/shrinking velocity where λ is stretching/shrinking rate. Two equal and opposite forces are introduced along the x-axis to stretch the wedge by keeping the origin fixed. The x-axis is the direction of the flow along the wedge and the y-axis normal to it. The lower part of the wedge is heated by hot fluid of the temperature T_f which provides a heat transfer coefficient h_f . At the wedge surface, a constant suction/injection is imposed.

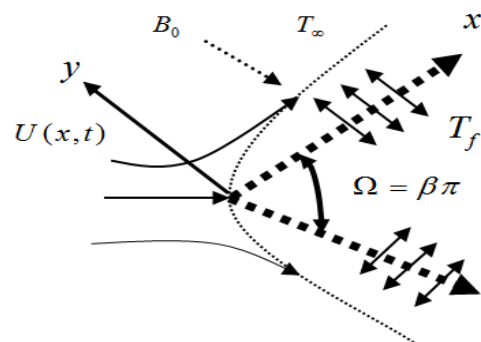


Fig 1: Flow Configurations and Coordinate System.

Under the above assumptions, the governing partial differential equations for this problem can be written as:

$$\frac{\partial N}{\partial t} + u \frac{\partial N}{\partial x} + v \frac{\partial N}{\partial y} = \frac{\nu_s}{\rho j} \frac{\partial^2 N}{\partial y^2} - \frac{s}{\rho j} \left(2N + \frac{\partial u}{\partial y} \right) \quad (3)$$

Energy Equation:

$$\frac{\partial T}{\partial t} + u \frac{\partial T}{\partial x} + v \frac{\partial T}{\partial y} = \frac{\kappa}{\rho c_p} \frac{\partial^2 T}{\partial y^2} + \frac{\mu}{\rho c_p} \left(\frac{\partial u}{\partial y} \right)^2 + \frac{\sigma B_0^2}{\rho c_p} (u - U)^2 \quad (4)$$

where $\nu_a = \frac{\mu + S}{\rho}$ is the apparent kinematic viscosity and $\nu_s = \left(\mu + \frac{S}{\rho} \right)_j$ is the spin-gradient viscosity.

Boundary Conditions

The boundary conditions for the above problem are

(i) On the surface of the wedge ($y = 0$):

$$u = \lambda U(x, t), \quad v = \pm v_w(x), \quad N = -n \frac{\partial u}{\partial y}, \quad -\kappa \frac{\partial T}{\partial y} = h_f (T_f - T) \quad (5a)$$

(ii) Matching with the free stream ($y \rightarrow \infty$):

$$u = U(x, t) = \frac{\nu x^m}{\delta^{m+1}}, \quad N = 0, \quad T = T_\infty \quad (5b)$$

where the constant $\lambda > 0$ corresponds to a stretching wedge and $\lambda < 0$ for a shrinking wedge while $\lambda = 0$ for a static wedge, $v_w(x, t)$ is the suction or injection velocity at the porous wedge where its sign indicates suction (< 0) or injection (> 0) and $U(x, t)$ is the potential velocity generated by the pressure gradient. The subscript f denotes the surface condition and the exponent m is known as Hartee pressure gradient parameter.

Non-Dimensionalization

The non-dimensional variables to obtain similarity solutions of the governing equations (1)-(4) under the boundary conditions (5a) and 5(b) are

$$\eta = y \sqrt{\frac{m+1}{2}} \sqrt{\frac{x^{m-1}}{\delta^{m+1}}}, \quad \psi = \nu \sqrt{\frac{2}{m+1}} \sqrt{\frac{x^{m+1}}{\delta^{m+1}}} f(\eta), \quad \theta(\eta) = \frac{T - T_\infty}{T_f - T_\infty}, \quad N = \nu \sqrt{\frac{m+1}{2}} \frac{x^{\frac{3m-1}{2}}}{\delta^{\frac{3m+3}{2}}} g(\eta)$$

(6) where η is the similarity variable and ψ is the stream function that satisfies the continuity equation (1).

Now substituting the equations (6) into equations (2)-(4) we obtain

$$(1 + \Delta) f''' + f f'' + \frac{2m}{m+1} (1 - f'^2) + \Delta g' - K[2 - 2f' - \eta f''] - \frac{2Ha}{m+1} (f' - 1) + \frac{2\theta}{m+1} \gamma = 0 \quad (7)$$

$$bg'' - \frac{2\Delta B}{m+1} (f'' + 2g) + fg' - \frac{3m-1}{m+1} f' + K(3g + \eta g') = 0 \quad (8)$$

$$\theta'' + \text{Pr } K \eta \theta' + \text{Pr } f \theta' + \text{Pr } Ec (f'')^2 + \frac{2}{m+1} Ha \text{Pr } Ec (f' - 1)^2 = 0 \quad (9)$$

where primes denote differentiations with respect to the variable η only.

The dimensionless parameters which appear in the above equations are as follows: $\gamma = \left(\frac{G_{rx}^2}{Re_x} \right)^{\frac{1}{2}}$ is the local buoyancy or free convection parameter. The case $\gamma \ll 1$ indicates free convection, $\gamma = 1$ indicates mixed convection and $\gamma \gg 1$ indicates forced convection, $\Delta = \frac{S}{\rho\nu}$ is the vortex viscosity parameter, $G_{rx} = \frac{g_0 \beta^* (T_f - T_\infty) x^3}{\nu^2}$ is the Grashof number, $Ec = \frac{U^2}{c_p (T_f - T_\infty)}$ is the Eckert number, $K = \frac{\delta^m}{\nu x^{m-1}} \frac{d\delta}{dt}$ is the unsteadiness parameter, $Ha = \frac{\sigma B_0^2 x}{\rho U}$ Hartmann number, $b = \frac{\nu_s}{\rho \nu j}$ is the spin gradient viscosity parameter, and $B = \frac{\delta^{m+1}}{j x^{m-1}}$ is the local micro-inertia density parameter.

The corresponding boundary conditions 5(a) and 5(b) becomes

$$f = f_w, f' = \lambda, g = -nf'', \theta' = Bi \sqrt{\frac{2}{m+1}} (\theta - 1) \text{ at } \eta = 0 \quad (10a)$$

$$f' = 1, \theta = 0, g = 0 \text{ at } \eta = \infty \quad (10b)$$

where $f_w = \pm v_w(x, t) \left(\frac{2}{m+1} \right)^{\frac{1}{2}} \frac{\delta^{\frac{m+1}{2}}}{\nu x^{\frac{m-1}{2}}}$ is the wall mass transfer coefficient which is positive

($f_w > 0$) for suction and negative ($f_w < 0$) for injection. $Bi = \frac{h_f}{\kappa} (Re)^{-\frac{1}{2}}$ is the Biot number.

Important Physical Parameters

The engineering parameters for the present problem are the local skin friction coefficient, local plate couple stress and local Nusselt number which can be expressed as

$$\frac{1}{2} C_{fx} Re^{\frac{1}{2}} = \sqrt{\frac{m+1}{2}} [1 + (1-n)\Delta] f''(0), M_{wx} = \frac{b(m+1)g'(0)}{(1+\Delta)B} \text{ and } N_{ux} Re^{-\frac{1}{2}} = Bi(1 - \theta(0)) \text{ respectively.}$$

NUMERICAL SOLUTION

Using the boundary conditions (10a) and (10b), the non-linear ordinary differential equations (7)-(9) have been solved numerically by applying sixth order Runge-Kutta method together with Nachtsheim-Swigert [13] shooting iteration technique with a set of prescribed physical parameter. $\Delta\eta = 0.001$ is the step size which was selected to be satisfactory for a convergence criterion of 10^{-6} in all cases. The value of η_∞ was found to each iteration loop by the statement $\eta_\infty = \eta_\infty + \Delta\eta$. The maximum value of η_∞ to each group of parameters $\gamma, \Delta, K, Ha, m, B, n, b, \lambda, Ec, Bi, Pr$, and f_w determined when the value of the unknown boundary conditions at $\eta = 0$ does not change to successful loop with an error less than 10^{-6} .

Code Verification

We have calculated the values of $f(\eta)$ and $f'(\eta)$ to find out the accuracy of present code where we have chose $\Delta = m = K = M = \gamma = 0$ for the present problem for the Falkner-Skan boundary layer equation. The data produced by the present code and that of White F. M. [14] are in excellent agreement that is shown in Table-1. This gives us enough confidence to use the present code for numerical calculations.

Table 1: Comparison of the Present Numerical Results with White [14] for Falkner-Skan Boundary Layer Flow when $\Delta = m = K = M = \gamma = 0$.

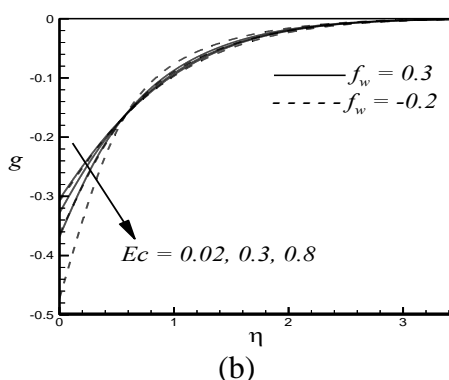
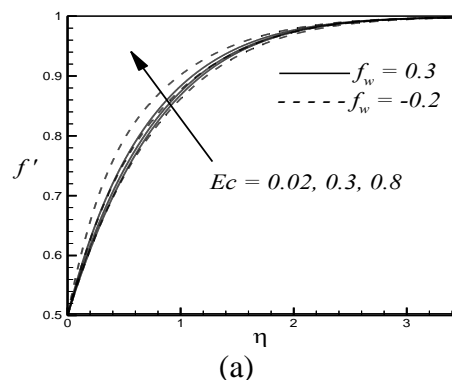
η	$f(\eta)$	$f(\eta)$	$f'(\eta)$	$f'(\eta)$
	Present work	White [15]	Present work	White [15]
0	0.0000	0.0000	0.0000	0.0000
1	0.2321	0.2329	0.4605	0.4606
2	0.8868	0.8868	0.8167	0.8166
3	1.7956	1.7955	0.9691	0.9690
4	2.7831	2.7838	0.9978	0.9977
5	3.7832	3.7832	0.9999	0.9999

RESULTS AND DISCUSSION

The Numerical results are obtained for different values of the physical parameters namely, the buoyancy parameter (γ), the unsteadiness parameter (K), microrotation parameter (n), suction/injection parameter (f_w), stretching/shrinking parameter (λ), viscous dissipation parameter or the Eckert number (Ec), Hartmann number (Ha), pressure gradient parameter (m), vortex viscosity parameter (Δ), spin-gradient viscosity parameter (b), micro-inertia density parameter (B) and Biot number (Bi) keeping Prandtl number $Pr = 21.0$ as fixed for micropolar fluid (see also Chato [15] and Valvano et al. [16]). The values of other parameters are chosen as $\gamma = 1$, $\Delta = 2$, $K = 0.5$, $m = 0.5$, $B = 0.5$, $b = 0.5$, $n = 0.5$, $Ha = 1$, $\lambda = 0.2$, $Ec = 0.2$ and $Bi = 0.5$. Since we have considered the mixed convection problem, the value of $\gamma = 1$ is taken throughout the calculation.

Figure 2(a-c), respectively, show the velocity, microrotation and temperature profiles for different values of Ec for both suction ($f_w > 0$) and injection ($f_w < 0$) cases. For the present study, we have considered viscous dissipation term to increase the motion of the fluid. From this term we obtained dimensionless parameter Ec . This parameter is called the motion controlling parameter. Figure 2(a) shows the velocity profiles increase with the increase of Ec for both suction and injection cases. Figure 2(b) shows the angular velocity remain negative and decrease with the increase of Ec within some domain $\eta \leq \eta_{critical}$ and increase

within the domain $\eta > \eta_{critical}$ for both suction and injection cases. The figure also shows that the angular velocity has a tendency to become positive as Ec increase for both cases. It is quite interesting to record the variation of microrotation near $\eta = 0.5$, where the profiles intersect each other. Another point is to note that microrotation profiles is dominated by suction than to injection up to $\eta = 0.5$ and then reverse effect is observed. Figure 2(c) shows the temperature profiles are quite significant for injection than to suction although temperature profiles increase with the increase of Ec for both suction and injection cases.



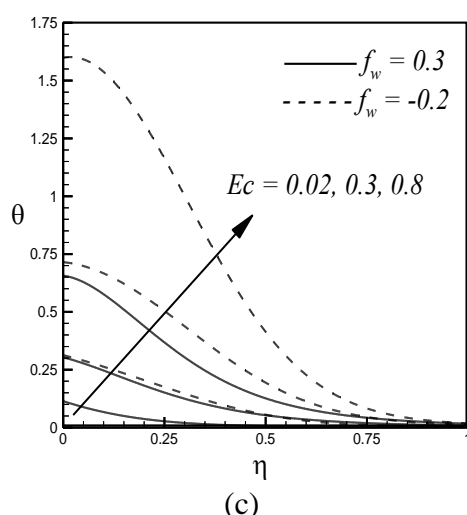


Fig. 2: Variation of Dimensionless (a) Velocity, (b) Microrotation and (c) Temperature Profiles for Different Values of Ec for both Suction and Injection Cases.

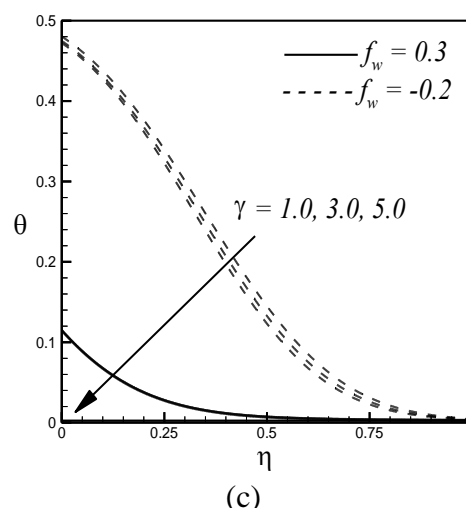


Fig. 3: Variation of Dimensionless (a) Velocity, (b) Microrotation and (c) Temperature Profiles of γ for both Suction and Injection Cases.

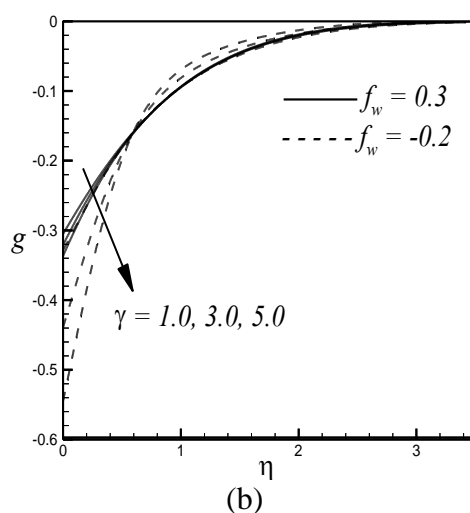
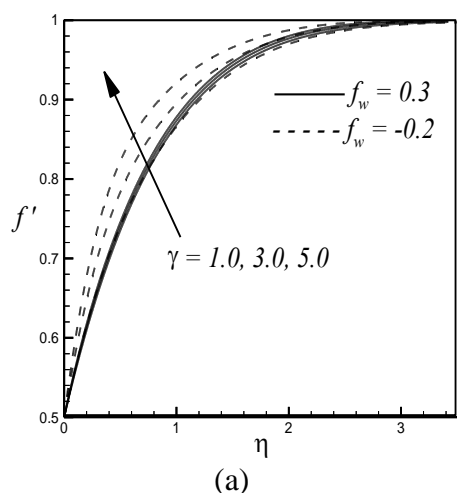


Figure 3(a) shows the velocity profiles increases with the increase of γ for both suction and injection cases and the increasing effects of velocity is higher when there is an injection at the surface of the wedge. Figure 3 (b) shows the angular velocity remain negative and decrease with the increase of γ within some domain $\eta \leq \eta_{critical}$ and increase within the domain $\eta > \eta_{critical}$ for both suction and injection cases. This figure also shows that for increasing values of γ the angular velocity has a tendency to become positive for both suction and injection cases. It is quite interesting to record the variation of microrotation near $\eta=0.5$, where the profiles intersect each other. Another point is to note that microrotation profiles is dominated by suction than to injection up to $\eta=0.5$ and then reverse effect is observed. Figure 3 (c) shows the temperature profiles decrease with the increase of γ for injection case while there is no change in temperature distributions for suction. In our results, it was found that for the increasing values of γ the fluid velocity increases and decrease the thermal boundary layer for the injection.

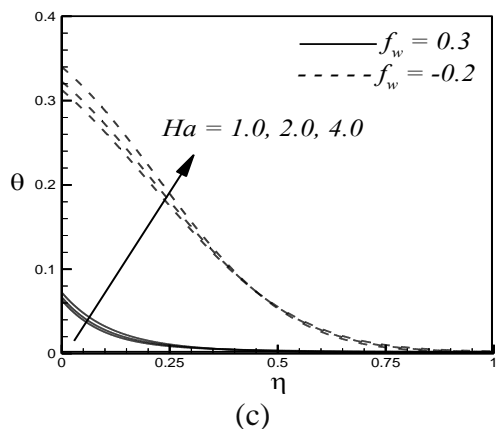
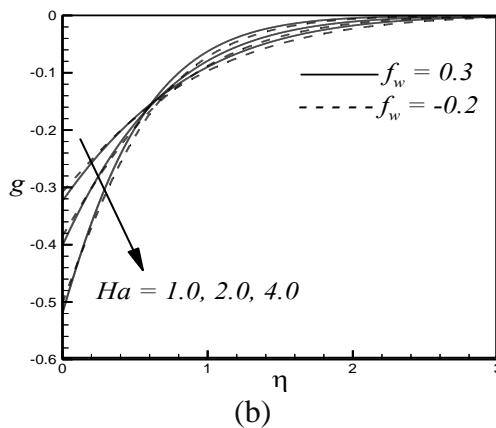
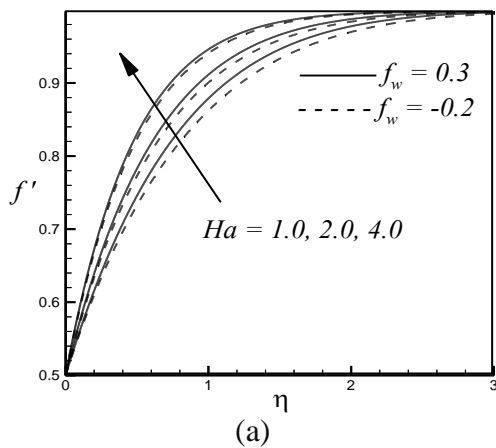
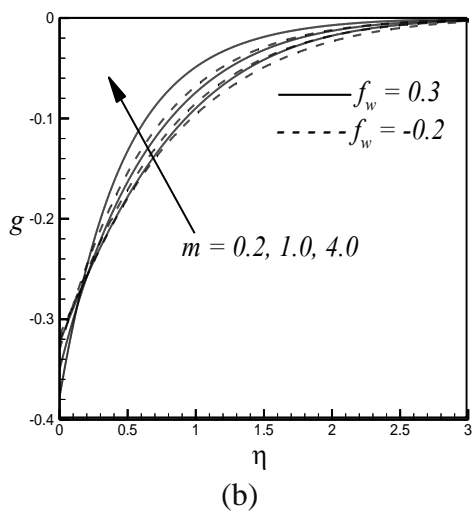
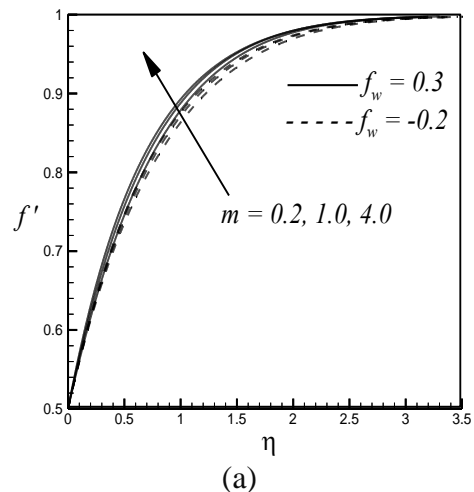


Fig. 4: Variation of Dimensionless (a) Velocity, (b) Microrotation and (c) Temperature Profiles for Different Values of Ha for both Suction and Injection Cases.

Figure 4(a) shows that the fluid velocity profiles increase with the increase of Ha for both suction and injection cases. This results also show that the velocity boundary layer thickness decreases with

the increase of Ha for both suction and injection which in turn increases the velocity gradient at the surface ($\eta=0$) and hence produce an increase in skin friction coefficient. Figure 4 (b) shows the dimensionless microrotation profiles remain negative and decrease with the increase of Ha within some domain $\eta \leq \eta_{critical}$ and increase within the domain $\eta > \eta_{critical}$ for both suction and injection cases. Figure 4 (c) shows the influence of Ha for the case of injection is quite significant and the temperature profile increase near the surface of the wedge with the increase of Ha for injection but for suction there is a negligible effect of temperature profiles.



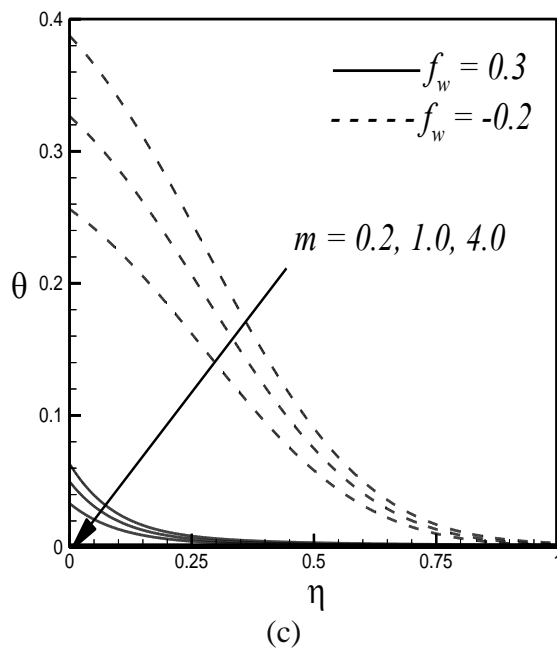


Fig. 5: Variation of Dimensionless (a) Velocity, (b) Microrotation and (c) Temperature Profiles for Different Values of m for both Suction and Injection Cases.

Figure 5(a), shows for increasing values of m , the fluid velocity increases for both cases. This figure also show that the increasing effect of velocity is higher for the case suction that to injection case. Figure 5 (b) depicts the non-dimensional microrotation profiles remain negative and increase with the increase of m within some domain $\eta > \eta_{critical}$ and the opposite phenomena occurs very near to the surface of the wedge for both suction and injection cases. This figure also shows that there is dominating effect of microrotation for suction than to injection after $\eta = 0.2$. Figure 5(c) shows temperature profiles decreases with the increase of m for both suction and injection cases whereas the decreasing effect of temperature is higher for an injection than to suction cases which means that injection more effective to decrease the fluid temperature. Therefore, a wedge angle parameter can be used to control the heat transfer characteristics of the fluid.

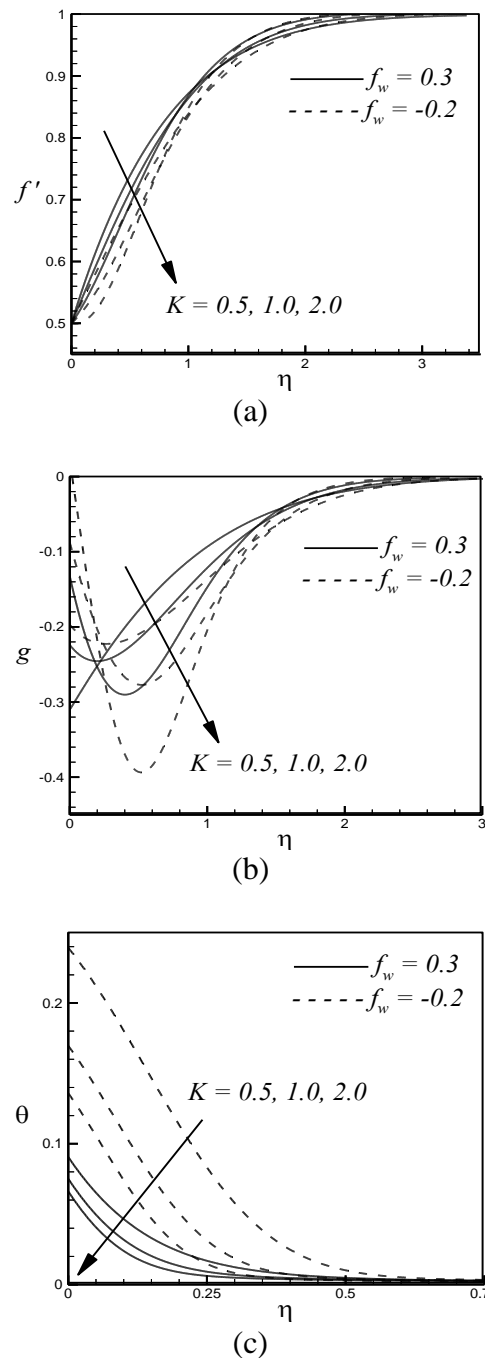


Fig. 6: Variation of Dimensionless (a) Velocity, (b) Microrotation and (c) Temperature Profiles for Different Values of K for both Suction and Injection Cases.

Figure 6(a) shows the velocity profiles decrease with the increasing values of K for $\eta \leq \eta_{critical}$ and increase away from the surface for both suction and injection cases. This figure also shows that there is tendency of a back flow phenomena for the increasing values of K near the surface

of the wedge for injection. Figure 6 (b) shows the microrotation in the boundary layer increases with the increase of κ in the vicinity of the surface of the wedge. But far away from the surface of the wedge where kinematic viscosity dominates the flow microrotation profiles overlap and decrease with the increase of κ for both suction as well as injection cases. This figure also shows that for the strong κ microrotation profiles become parabolic in shape for both suction and injection cases. Figure 6 (c) shows the non-dimensional temperature profiles within the boundary layer decrease with the increase of κ for both suction as well as injection cases but temperature field has a large decreasing effect for injection than to suction.

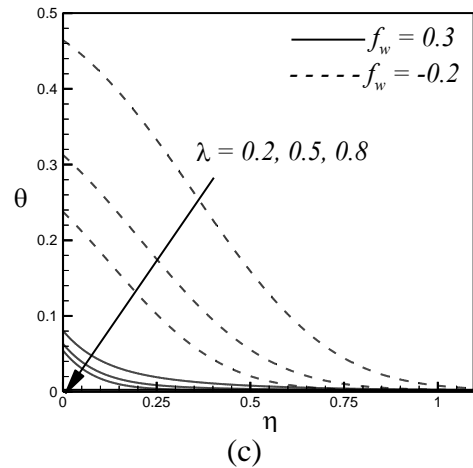
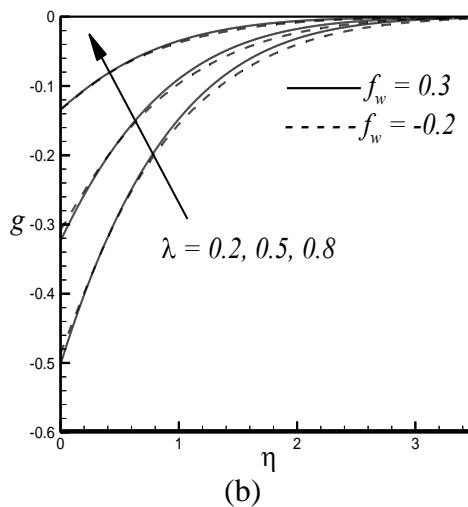
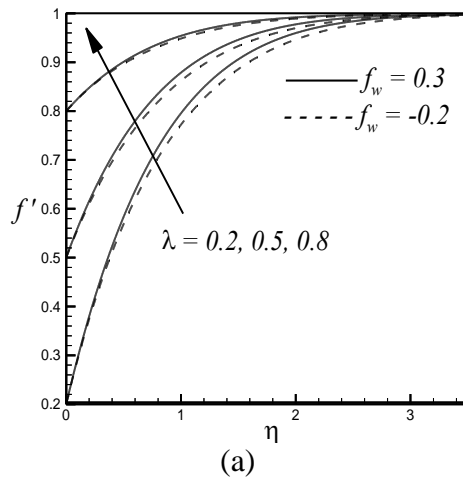


Fig. 7: Variation of Dimensionless (a) Velocity, (b) Microrotation and (c) Temperature profiles for $\lambda > 0$ for both Suction and Injection Cases.

Figure 7(a) shows that the fluid velocity profiles increase with the increase of $\lambda (> 0)$ for both suction and injection cases. Figure 7(b) shows the angular velocity remain negative and increase with the increase of $\lambda (> 0)$ for both suction and injection cases. This figure also show that as $\lambda (> 0)$ increases the angular velocity has tendency to become positive for both suction and injection cases. Figure 7(c) shows the temperature profiles decreases with the increase of $\lambda (> 0)$ for both suction and injection cases but there is a dominating effect of temperature profiles for injection than to suction.

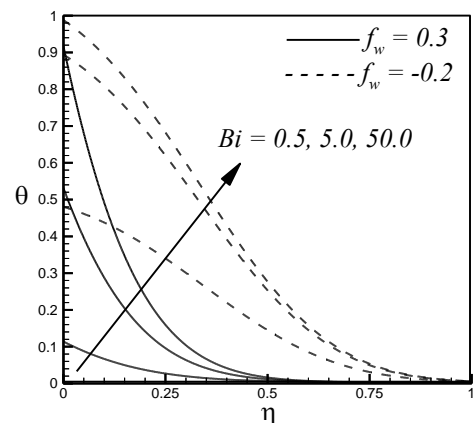


Fig. 8: Variation of Dimensionless Temperature Profiles for Different Values of Bi .

Figure 8 shows the temperature profiles for different values of the Biot number or surface convection parameter Bi for both suction and injection cases. This figure illustrate that temperature distribution is higher for injection than to suction though the temperature profiles within the boundary layer increase with the increase of Bi for both suction and injection cases. Therefore, to increase the temperature of the fluid injection is more efficient than suction.

Table: 2: Numerical Values of the Local Skin-Friction Coefficient, Plate Couple Stress and the Local Nusselt Number for Different Values of Ha and Ec .

Ha	Ec	$f''(0)$	$g'(0)$	$-\theta'(0)$
0	0.2	0.676317	0.260862	0.138559
	0.3	0.691294	0.276138	0.180395
	0.5	0.721976	0.307504	0.268369
	0.8	0.767578	0.355289	0.409431
	1.0	0.798957	0.388406	0.511006
1	0.2	1.061710	0.628291	0.295958
	0.3	1.089368	0.660719	0.416474
	0.5	1.143586	0.724742	0.660008
	0.8	1.222832	0.819296	1.034878
	1.0	1.274408	0.881631	1.290999
2	0.2	1.322954	0.907064	0.403786
	0.3	1.355812	0.947742	0.577786
	0.5	1.410032	1.027693	0.927468
	0.8	1.513050	1.144358	1.457579
	1.0	1.573365	1.220923	1.876097

Table 2 shows the influence of physical parameters Ha and Ec on the skin friction coefficient or rate of share stress, the plate couple stress and rate of heat transfer. It is clear that the Eckert number has an increasing effect on the skin friction coefficient or rate of share stress, the plate couple stress and rate of heat transfer for both suction as well as injection. From this table it is interesting to observe that an increase in Ha produce the skin friction and heat transfer rate. The increase of skin friction is due to the increase of Ha , which may be attributed to the fact stated earlier that an increasing Ha is comparable to increasing the flow viscosity, which leads to skin friction increase.

Table 3: Numerical Values of the Local Skin-Friction Coefficient, Plate Couple Stress and the Local Nusselt Number for Different Values of f_w , m and γ .

f_w	m	γ	$f''(0)$	$g'(0)$	$-\theta'(0)$
0.5	0.2	1	1.06171	0.62821	0.29595
		2	1.18322	0.76998	0.30121
		3	1.30077	0.90887	0.30677
	0.5	1	1.08455	0.75013	0.26984
		2	1.17369	0.85674	0.27547
		3	1.26055	0.96204	0.28044
	1.0	1	1.11051	0.88706	0.24367
		2	1.17060	0.96059	0.24871
		3	1.23047	1.03434	0.25306
-0.2	0.2	1	1.43518	0.65812	1.99258
		2	2.20283	1.25839	2.52974
		3	3.70066	2.52265	4.06777
	0.5	1	1.32938	0.65939	1.88571
		2	1.88470	1.11073	2.27073
		3	2.70255	1.82462	3.01868
	1.0	1	1.23280	0.66583	1.77920
		2	1.61067	0.98192	2.04411
		3	2.09499	1.41053	2.46096

Table 3 shows the influence of physical parameters m and γ on the skin friction coefficient or rate of share stress, the plate couple stress and rate of heat transfer while other parameters are fixed. It is clear that the wedge angle parameter m has an increasing effect on the skin friction coefficient, the plate couple stress and rate of heat transfer for both suction and injection cases. From this table it is interesting to observe that the rate of heat transfer increase with the increase of γ whereas decrease with the increasing values of m for both suction and injection cases. For the increasing values of buoyancy parameter, which increases the wall shear stress hence increasing the skin friction coefficient. This is a consequence of the existence of a favorable pressure gradient above the surface of the wedge due to the buoyancy effects. It is also seen that a higher rate of heat transfer is observed when there is injection at the surface of the wedge.

CONCLUSION

The behavior of unsteady MHD mixed convective mass flow and heat transfer of micropolar fluid over a permeable shrinking/stretching wedge with viscous dissipation and Joule heating is investigated numerically. The numerical results have been presented in the form of graphs and tables. Important findings of this investigation are given below:

1. The fluid velocity inside the boundary layer increases with the increasing values of Eckert number as well as Hartmann number.

NOMENCLATURE

B_0	Uniform magnetic field
Bi	Biot number
b	Spin gradient viscosity parameter
B	Vortex viscosity parameter
Cf_x	Skin- friction coefficient
C_p	Specific heat at constant pressure
f	Dimensionless stream function
F_w	Dimensionless suction/injection parameter
g	dimensionless microrotation
h_f	Heat transfer coefficient
j	Micro -inertia density
K	Unsteadiness parameter
M	Magnetic field parameter
m	Wedge angle parameter
M_{wx}	Plate couple stress
n	Microrotation parameter
N_{ux}	Nusselt number
Pr	Prandtl number
Re	Local Reynolds number
S	Microrotation coupling coefficient
T	Temperature of micropolar fluid within boundary layer
T_f	Temperature at the sheet (surface)
T_∞	Temperature of the ambient fluid

REFERENCES

1. Eringen A.C. *Theory of micropolar fluids*. J. Math. Mech. 1966, 16, 1-18p.
2. Eringen A.C. *Theory of thermomicropolar fluids*. J. Math. Anal. Appl. 1972, 38, 480-496p.

2. The angular velocity decreases with the increasing values of Eckert number, buoyancy parameter as well as wedge angle parameter.
3. The temperature distribution increases with the increasing values of Eckert number, Biot number whereas it decreases with an increasing value of the wedge angle parameter.
4. The rate of shear stress and the rate of heat transfer increase with the increasing values of Hartmann number and Eckert number.

Greek Symbols

v	Velocity along x-axis
v_0	Suction/injection velocity
x	Coordinate along the plate
y	Coordinate normal to the plate
ρ	Density of the fluid
μ	Coefficient of dynamic viscosity
ν_a	Apparent kinematic viscosity
μ_s	spin-gradient viscosity
ν_∞	Kinematic coefficient of viscosity with constant property
N	Microrotation component
κ	Thermal conductivity
η	Similarity parameter
τ_w	Wall shear stress
θ	Dimensionless temperature
Δ	Vortex viscosity parameter (micropolar parameter)
ψ	Stream function
$\Delta\eta$	Step size
u	Velocity along x-axis

Subscripts

f	Refers to conditions at the wall
-----	----------------------------------

Superscripts

m	Velocity exponent
-----	-------------------

3. El-Hakim M.A. Mohammadein A.A., El-Kabeir S.M., Gorla R.S. *Joule heating effects on magnetohydrodynamic free convection flow of a micropolar fluid*. International communications in heat and mass transfer. 1999, 26(2), 219-

- 27p.
4. Duwairi H.M. *Viscous and Joule heating effects on forced convection flow from radiate isothermal porous surfaces*. Int. J. Numer Meth. Heat Fluid Flow. 2005, 15, 429-440p.
5. Partha M.K., Murthy P.V.S.N., Rajasekhar G.P. *Effects of viscous dissipation on the mixed convection of heat transfer from an exponential stretching surface*. Heat and Mass Transfer. 2005, 41, 360-366p.
6. Ishak A., Nazar R., Pop. *Falkner-Skan equation for flow past a moving wedge with suction or injection*. Journal of Applied Mathematics and Computing. 2007, 25(1-2), 67-83p.
7. Rahman M.M. *Convective flows of micropolar fluids from radiate isothermal porous surface with viscous dissipation and joule heating*. Common Nonlinear Sci Numer Simulat. 2009, 14, 3018-3030p.
8. Aissa W.A., Mohammadein A.A. *Joule heating effects in a micropolar fluid past a stretching sheet with variable electric conductivity*. J. Comput. Appl. Mech. 2005, 6, 3-13p.
9. Kishan. N., Reddy S.B. *MHD flow and heat transfer of a non Newtonian power-law fluid past a stretching sheet with suction/injection and viscous dissipation*. International Journal of Applied Mathematical Research. 2012, 1(4), 681-705p.
10. Alam M.S., Sattar M.A., Rahman M.M., Postelnicu A. *Local similarity solution of an unsteady two-dimensional MHD convective flow of a micropolar fluid past a continuously moving porous plate under the influence of magnetic field*. Int. J. Heat and Technology. 2010, 28(2), 95-105p.
11. Osalusi E, Side J, Harris R, Johnston B. *On the effectiveness of viscous dissipation and Joule heating on steady MHD flow and heat transfer of a Bingham fluid over a porous rotating disk in the presence of Hall and ion-slip currents*. Int. Com Heat Mass Trans. 2007, 34, 1030-40p.
12. Su X., Zheng L., Zhang X., Zhang J. *MHD mixed convective heat transfer over a permeable stretching wedge with thermal radiation and ohmic heating*. Chemical Engineering Science. 2012, 78, 1-8p.
13. Nachtsheim P.R., Swigert P. *Satisfaction of the asymptotic boundary conditions in numerical solution of the system of non-linear equations of boundary layer type*. NASA TND-3004. 1965.
14. White F.M. *Viscous Fluid Flows*. Third Edition, McGraw-Hill, New York, 2006.
15. Chato J.C. *Heat transfer to blood vessels*. J. Biomech Eng. 1980, 102(2), 110-118p.
16. Valvano J.W., S Nho, Anderson G.T. *Analysis of the WeibaumJiji model of blood flow in the canine kidney cortex for self-heated thermistors*. J. Biomech Eng. 1994, 116(2), 201-207p.